2012

New Correlations for the Air-Side Heat Transfer Coefficient of Microchannel Heat Exchangers Under Quasi-Steady State Frosting Operating Conditions

Ehsan Moallem
moallem@okstate.edu

Lorenzo Cremaschi

Daniel E. Fisher

Developing Empirical Correlations for Frost Thickness and Air Face Velocity Degradation for Microchannel Heat Exchangers Used in Heat Pump Applications under Frosting Condition

Ehsan Moallem[1]*, Tommy Hong[1], Lorenzo Cremaschi[1], Daniel E. Fisher[1]

[1] School of Mechanical and Aerospace Engineering, Oklahoma State University, Stillwater, OK, 74078, USA

* Corresponding Author
(Phone: +1 405 762 3393, email: moallem@okstate.edu)

ABSTRACT

This study experimentally investigated the frost growth on louvered folded fins in outdoor microchannel heat exchangers used in air-source heat pump systems. The effects of surface temperature and fin geometries on the performance of the microchannel heat exchangers under frosting condition were studied. 7 fin samples with various fin width, fin height and fin density were tested in controlled laboratory conditions that replicated those of actual heat pump systems in winter season. The fin surface temperature was experimentally estimated with the novel methodology developed in the present study. Experimental data of local frost thickness, air pressure drop across the coils, time of frost-defrost cycles and heat transfer rates were recorded for heat exchangers operating in actual transient frosting conditions. Data showed that the frosting time and the frost growth rates were depended mainly on the local fin surface temperature. A set of empirical correlations were developed to predict the frost thickness on fin leading edge and the reduction of air face velocity due to air pressure drop across the frosted coil during frosting operation. The correlations aid to calculate the instantaneous air-side Reynolds numbers during frosting operation of the fin samples. These are critical for predicting the heat transfer rates of the microchannel coils in quasi-steady state frosting operating conditions.

1. INTRODUCTION

Air source heat pump systems are used for heating and cooling of residential and commercial buildings all year around. Their outdoor coils accumulate frost on their surface in winter operation mode and defrost cycles need to be periodically executed in between the heating cycles. Microchannel coils have been employed recently in heat pump applications to replace conventional fin and tube coils due to their compactness, lower coil weight and less refrigerant charge which could lower the direct contribution to global warming due to potential refrigerant leakage (Garimella, 2003; Kim and Groll, 2003; Kim and Bullard, 2002; Park and Hrnjak, 2007). During heating mode, the energy performance of heat pump systems with microchannel outdoor coils are generally low due to a higher frequency of defrost cycles (Kim and Groll, 2003; Padhmanabhan et al., 2008).

There are several parameters that affect frost formation on outdoor coils, such as air velocity, air humidity, air temperature, cold surface temperature (Kondepudi and O'Neal, 1989; Lee et al., 1997) surface energy and fin-base surface microscopic characteristics (include coatings and roughness) (Na and Webb, 2003; Shin et al., 2003), fin geometry and coil water retention after defrost cycles (Xia et al., 2006).

Kim and Groll (2003) studied two microchannel geometries with different fin density and coil orientations under frosting condition and concluded that water drainage and refrigerant distribution in headers needed to be improved for achieving a better frosting performance. Xia et al. (2006) investigated five louvered-fin flat tube microchannel evaporators experimentally and observed that water retention has a significant effect on the air pressure drop in the next cycles. In another study, Zhang and Hrnjak (2010) investigated frosting performance of parallel-flow parallel-fin (PF^2) flat tube microchannel heat exchangers with horizontally installed tubes. The authors observed an improvement in frosting performance over a conventional serpentine fin which was attributed to better drainage capability of the PF^2 heat exchanger. Padhmanabhan et al. (2008), on the other hand, observed that removing the water residual at the end of the defrost cycle by flushing the microchannel coil with pressurized nitrogen improved

the next frost cycle time by only 4%. The preliminary results of this study (Moallem et al., 2012a) also showed that water retention, which was assumed to be one of the main reasons of faster frost growth on microchannels, is not the dominant factor affecting the frost, even though it seems to have some effects on the air side pressure drop. The key parameters that affect frost nucleation and growth were observed to be fin surface temperature (Moallem et al., 2012a) and the fin geometry. In several previous studies on microchannel heat exchanger in the literature, the geometries were varied to search for the best option for thermal performance. As a result, the effect of geometry modification was coupled with the effect of surface temperature change. To isolate and study the effect of surface temperature, a new methodology was developed by the authors that measured and controlled the fin surface temperature independently and isolated its effects from the geometry effects (Moallem et al., 2012c). The experimental data of authors' previous work are used in the present study.

Although a number of studies are available on frosting behavior of microchannels, their findings are limited to a limited number of geometries tested. The essence of developing an empirical correlation aims to unite previous findings into a general form that could be employed for a variety of geometries. The most important correlations that would be needed are for the frost thickness, instantaneous air face velocity, and instantaneous heat transfer coefficient. In the present study, new correlations for frost thickness correlation and the reduction of the air face velocity are developed and discussed. The correlations were verified against experimental data. . The scientific merit of this work is a fundamental understanding of frost growth, which changes the air side hydraulic geometry for the various geometries of folded louvered fins of microchannel heat exchangers. Once the instantaneous hydraulic geometry and air velocity are determined during the frost period, the Reynolds numbers are calculated. These numbers could be used for the development of instantaneous heat transfer coefficients during frosting operation, which is a future extension of this work.

2. EXPERIMENTAL SETUP

The fin samples are one column of louvered fins (15 cm in length) cut from commercially available microchannel coils. The tubes of this one column were eliminated and heat conduction was adopted in cooling the samples. This approach helped to eliminate the effect of different internal tube designs and microchannel ports and ensured a uniform one dimensional conduction heat transfer. A typical fin sample and schematic can be seen in Figure 1. The detail geometry of the samples is shown in Table 1.

In order to remove the heat from the sample fin, or cool it to the desired temperature, a method originally proposed by Thomas et al. (1999) was used. ThermoElectric Cooling (TEC) modules were installed, in each side of the samples to remove the heat and control the fin temperature as shown in Figure 2. With this configuration, thermocouples at the base of the fins samples showed a constant temperature of about -5, -8 and -11°C in each test. An air flow test set up was designed and built in laboratory to control the test condition specified in (AHRI, Standard 210/240, 2008) for heat pump system performance rating. The apparatus and the vice that holds the sample were placed inside a large air tunnel as shown in step 4 at the top and component 2 at the bottom of Figure 2. The tunnel is a close loop duct system equipped with ultrasonic humidifiers, refrigeration coil, electrical heater, and a centrifugal variable speed fan. The inlet air is controlled at 1.67/0.56°C (35/33°F) dry bulb/wet bulb temperature (~82% RH).

All experimental tests were conducted with the fin sample initially in dry condition. Each test started with air at 1.5m/s face velocity on fin samples. Fan was kept at constant RPM throughout the entire test and air face velocity was allowed to drop. This method of testing was preferred over a constant air velocity method since it was closer to the actual operation of the outdoor evaporator coils in air-source heat pump systems. More details about experimental setup can be found in Hong et al. (2012).

Frost thickness was measured with a magnifying high resolution CCD (Charge-Coupled Device) camera that has a borescope probe. The value of frost thickness was obtained by scaling high resolution images using special imaging computer software (iView PC) with an accuracy of ±0.03mm. The uncertainty was calculated using uncertainty propagation calculation which showed 12% on air side and 8% on conduction side. More details about the instrumentation and test procedures are in Hong (2011) and Hong et al. (2012). The verifications of the instrumentation connectivity, accuracy and validation of proper data recording were demonstrated through a set of validation tests called calorimeter tests. Experimental validation tests included the heat balance verification (two methods of air enthalpy method vs. conduction heat transfer), performed on all of the fin samples which showed the difference never exceeded 15% in dry tests and during quasi steady state periods of the frosting tests (Moallem et al., 2012d).

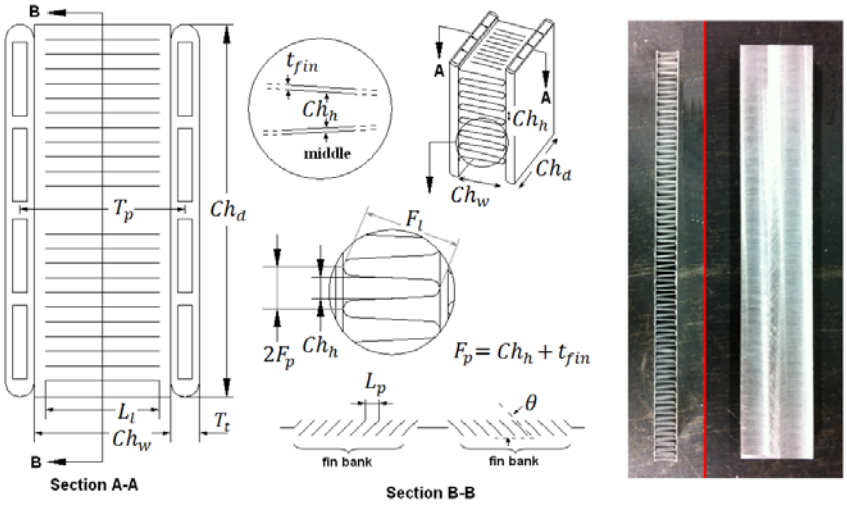

Figure 1: Schematic drawing of a microchannel sample with geometrical parameters shown in the left side of the figure. (These drawings were made at Oklahoma State University and they were not given by the manufacturers). One of the fin samples is shown on the right side of the figure**.**

Table 1: Details of the geometries of the microchannel fin samples used in the present study

Sample No.	Fin Depth (Ch_d) (mm)	Fin Width (Ch_w) (mm)	Channel Height (Ch_h) (mm)	Fin Density (FPI)	Tube thickness (mm)	Fin Thickness (mm)	Fin type	No of louvers	Louver pitch (mm)	Louver angle (Deg)	Louver Height (mm)	Louver Length (mm)
1	27.0	8.0	2.34	10.4	1.8	~0.1	Flat fin corrugated	-	-	-	-	-
2	27.0	8.0	1.77	13.6	1.8	~0.1	Louvered	16	1.50	~30	0.22	6.5
3	26.0	7.6	1.15	20.3	1.4	~0.1	Louvered	24	0.94	~30	0.09	6.0
4	25.0	10.0	1.21	19.4	1.7	~0.1	Louvered	18	1.22	~30	0.24	7.5
5	25.0	13.0	1.20	19.6	2.0	~0.1	Louvered	20	1.23	~30	~0.21	9.5
6	30.0	8.1	1.27	18.5	1.4	~0.1	Louvered	28	0.86	~30	~0.2	7.0
7	19.0	8.0	1.36	17.4	3.0	~0.1	Louvered	16	0.94	~30	~0.2	6.5

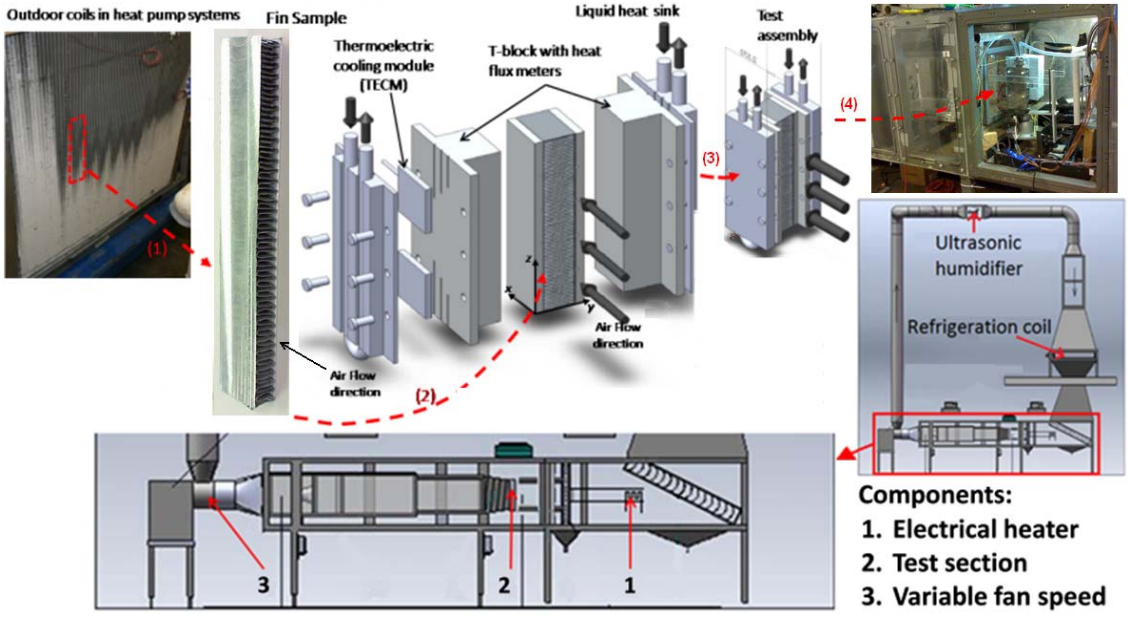

Figure 2: Procedure for the preparation of the test assembly set up inside the wind tunnel (top) and schematic of air tunnel or airflow loop (bottom).

3. RESULTS AND DISCUSSION

3.1 Visual Observations

Frost growth pattern on microchannel fin sample 2 is shown in Figure 3. Similar results were observed for other samples (Moallem et al., 2012c). The location of the camera was in the center of the 6 inch long sample. Figure 3 shows the frost accumulation over time; the frost time is measured from the time the air flow was started on the cold sample to the end of the frosting period, that is, when the air face velocity reached 30% of its initial value. There were not significant visual differences between the frost layers that grow on different geometries. The end of the cycle occurred at a time when the air gaps between the fins were almost completely blocked by frost.

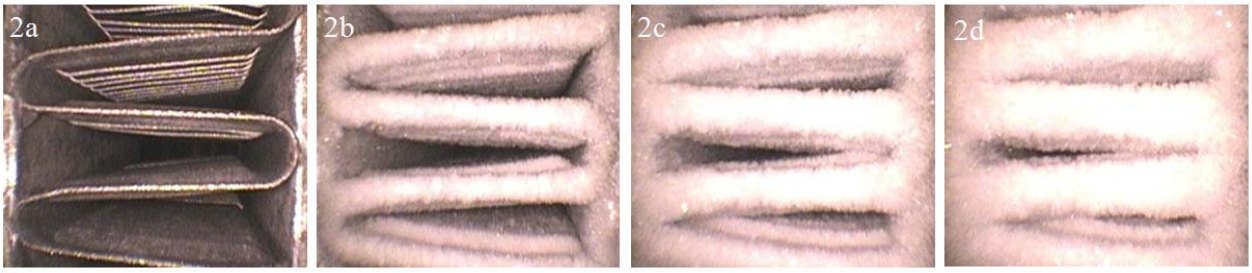

Figure 3: Microchannel sample 2 under frosting conditions. a, b, c and d represents time of 0, 8, 16 and 24 minutes after starting the test. T_{surf}= -8°C and air temperature=1.7°C/0.6°C db/wb. Similar visual results were observed for surface temperatures of -5°C and -11°C with different time duration.

3.2 Frost Empirical Correlation, Scope and Fundamentals

The effect of various surface temperatures and geometry were previously published in authors previous work (Moallem et al., 2012c). In this section, a new set of frost correlations were developed and verified against experimental data. The fundamental frost formation theories in the literature associated the frost formation rate with vapor pressure of the air and temperature at which frost forms, which is basically the surface temperature. In crystallization theory, for the phase transition of the water vapor into ice crystals, air should be in a supersaturation level. Air supersaturation (in this paper we refer to this quantity as frost number, Fs) is the driving force for migration of water vapor particles and their deposition on the cold surface which is defined as the following (Na and Webb, 2004; Sanders, 1974):

$$Fs = S = \frac{P_{air} - P_{surf}}{P_{surf}} \tag{1}$$

$$\delta = f(t_t, T_{surf}, T_{air}, \omega_{air}, Geometry) \Rightarrow \delta = f(Fo, Fs, Geometry) \qquad Geometry: Ch_w, Ch_h, Ch_d \tag{2}$$

$$\delta = \frac{t}{(Ch_h/2)} \tag{3}$$

δ is dimensionless frost thickness and is unity when the free flow area between two adjacent fins is completely blocked by frost. As data on Figure 4 shows, the frost thickness starts from 0 at the beginning of the test and reaches near 1 at the end. For geometry parameters, we observed that except than a few discrepancies, three parameters of fin pitch (or Ch_h), fin length (Ch_w) and fin depth (Ch_d) (as shown in Figure 1) could predict the experimental data within sufficient accuracy.

3.3 Frost Thickness Correlation

In order to predict the frosting behavior of microchannels, it should be pointed out that the air side free flow geometry changes during frost period. This observation is the key to calculate the correct instantaneous Reynolds number in quasi-steady state operation. Although the frost thickness was measured only at the leading edge, this parameter is sufficient to calculate the critical Reynolds number, which is the Re number estimated at the minimum cross section area. The authors of the present paper concluded that some of the geometrical parameters in the frost thickness correlation had to be in dimensional form in order to provide better accuracy of correlation when compared to the experimental data. Minimizing root mean square errors was the approach taken to find the coefficients of the correlation, which is as follows:

$$\delta = \alpha \, Fo_m{}^{\beta} \tag{4}$$

$$Fo_m = \frac{D_{ab} t_t}{Ch_h^2} \tag{5}$$

$$\alpha = \left(\frac{1}{\beta^{5.5}}\right)\left(c_1 Ch_w{}^2 + c_2 Ch_w + c_3\right)\left(c_4 Ch_h{}^2 + c_5 Ch_h + c_6\right)\left(c_7 Ch_d{}^2 + c_8 Ch_d + c_9\right)(Fs - c_{10}) + \left(c_{11} Ch_w{}^2 + c_{12} Ch_w + c_{13}\right)\left(c_{14} Ch_h{}^2 + c_{15} Ch_h + c_{16}\right)\left(c_{17} Ch_d{}^2 + c_{18} Ch_d + c_{19}\right) \tag{6}$$

$$\beta = 0.75 + \left(c_{20} Ch_w{}^2 + c_{21} Ch_w + c_{22}\right)\left(c_{23} Ch_h{}^2 + c_{24} Ch_h + c_{25}\right)\left(c_{26} Ch_d{}^2 + c_{27} Ch_d + c_{28}\right)(Fs - c_{10}) \tag{7}$$

In above equations α and β are functions of geometry and Frost number. α ranges from 1.2E-5 to 1.9E-3 and β varied from 0.55 to 0.99. Ch_h, Ch_w and Ch_d have dimensions in mm. The coefficients c_1 to c_{28} are constants and their values are shown in Table 2. Equation (4) was able to capture the experimental data of frost thickness on 21 different frost data that included 7 different geometries tested at 3 fin surface temperatures. A comparison of the instantaneous frost predicted by using equation (4) vs. experimental thickness data for sample 6 and sample 2 at three temperatures is shown in Figure 4. Similar results were observed for other geometries (Figure 5).

Table 2: Coefficients of geometry in general frost thickness correlation

c1	-2.24444E-06	c6	-2.16158E+00	c11	-3.82446E-07	c16	-1.62560E+00	c21	-5.555E-01	c26	-1.099E-02
c2	4.34942E-05	c7	2.47364E-03	c12	-6.77335E-06	c17	-2.86864E-03	c22	4.275E+00	c27	5.164E-01
c3	-7.89706E-05	c8	-1.03390E-01	c13	2.58664E-04	c18	1.33878E-01	c23	1.619E+00	c28	-5.848E+00
c4	-1.22951E+00	c9	1.96625E+00	c14	-9.36590E-01	c19	-5.38708E-01	c24	-5.678E+00		
c5	4.16146E+00	c10	1.36432E+00	c15	3.35870E+00	c20	1.28500E-02	c25	6.102E+00		

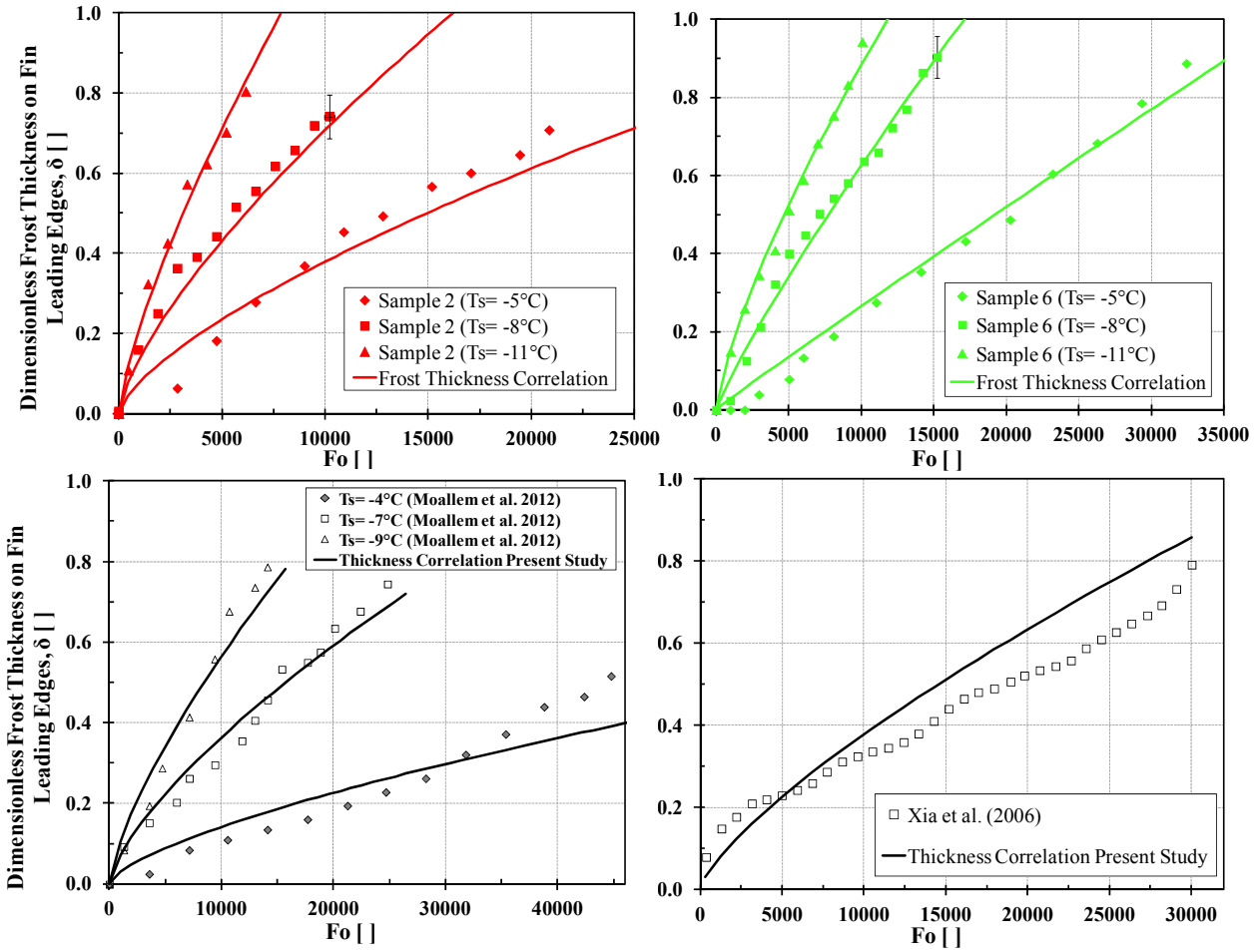

Figure 4: Frost thickness correlation versus experimental measured frost thickness data for Sample 2 and 6 (top). Similar results were observed for other samples. Comparison of present correlation with previous published works Moallem et al. (2012a) and Xia et al. (2006) (bottom).

The developed correlation was also compared to other experimental microchannel frost thickness data with larger 1ft by 1ft microchannel coils (Moallem et al., 2012a) and the result was in satisfactory agreement as shown in Figure 4. Also the present form of correlation was compared against frost thicknesses data obtained in the literature (Xia et al., 2006). In their work, Xia et al. used a different experimental setup to measure frost growth but the frost thickness correlation developed in this work captured well the trend of the data, as shown in Figure 4. It should be emphasized that the coefficients c_1 to c_{28} in Table 2, which were based only on the measurements of Hong et al. (2012), were not tuned to fit the experimental results of Moallem et al. (2010) and Xia et al. (2006).

The overall performance of frost correlation is shown in Figure 5 in which frost thickness ratios $\delta_{correlation}/\delta_{experimental}$ is shown on vertical axis versus the actual frost thickness measurement data. The correlation seems to be able to predict the experimental frost thickness reasonably well for all of data. However there are some data points that have significant deviation from correlation prediction when the frost thickness ratio is less than 0.2. This is due to the early condensation frosting or formation of supercooled droplets which delayed frost growth process at early stages of growth as discussed in details in previous studies (Hoke et al., 2004; Moallem et al., 2012b; Na and Webb, 2003). These points acted like singularity points and created division by zero, and thus large errors, in the analysis.

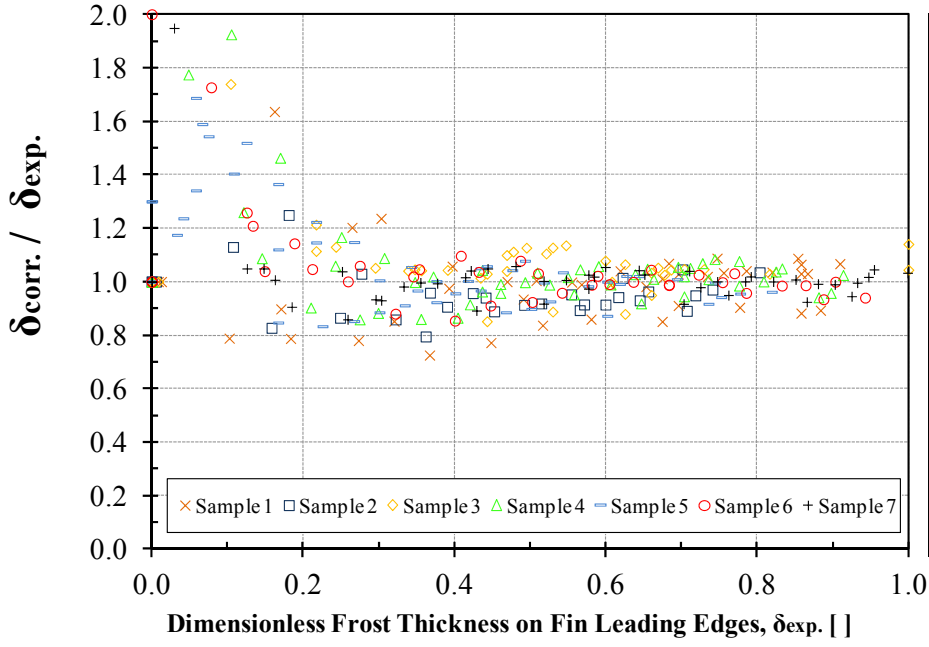

Figure 5: Frost Thickness Correlation versus experimental measured dimensionless frost thickness data for Samples 1 ~ 7.

Sample No./ Bank	δ predicted within average of ± [%]	RMS Error [%]
Sample 1	17.4	50.4
Sample 2	11.5	21.5
Sample 3	26.4	34.7
Sample 4	29.0	38.8
Sample 5	16.4	28.4
Sample 6	16.2	28.2
Sample 7	6.5	13.4
80% of Entire Data Base	5.2	-
95% of Entire Data Base	9.8	-
Entire Data Base	17.6	30.8

Table 3: Thickness Correlation overall performance

The error analysis has been performed on the present frost thickness correlation and relative errors and RMS (Root Mean Square) errors have been reported in Table 3. The relative error indicates that the frost thickness correlation can predict the experimental data within a certain average percentage of accuracy calculated according to the following:

$$\text{Relative Error} = \frac{1}{n}\sum \frac{\text{ABS}(\delta_{corr.}-\delta_{exp.})}{\delta_{exp.}} \times 100 \qquad \text{RMS Error} = \sqrt{\frac{1}{n}\sum \left(\frac{\delta_{corr.}-\delta_{exp.}}{\delta_{exp.}}\right)^2} \times 100 \qquad (8)$$

In which n is the total number of data points, which is 320 point in the present study. RMS error was calculated using the same approach. As data in Table 3 shows, the present frost thickness correlation predicts the entire set of experimental data with average ±17.6% accuracy. As discussed before with eliminating the points of singularity which frost has a near zero values at those points, the correlation can predict 95% of the thickness experimental data within average of ±9.8% accuracy.

3.4 Air Face Velocity Degradation Correlation

In dry and wet microchannel coils the geometry can be assumed to be fixed and steady state conditions are sound. In frosting conditions the geometry is changing at each moment and the velocity is the result of the pressure balance across the coil and to the additional resistance created by the frost buildup on the coil surfaces. As the frost grows, the free flow area between fins is reduced. The increased air pressure drop causes a major reduction in air face velocity. It is also possible to force the air face velocity to remain constant all through a frost test by increasing the fan rotational speed and fan power. This second approach is quite different from the actual operation of outdoor coils of air-source heat pumps. In addition, our calculations showed that forcing the air face velocity to be constant would cause the local air velocity in between the frosted fins to increase by more than 10 times with respect to initial dry conditions. The authors concluded that constant air face velocity would provide unrealistic heat transfer coefficients and very large heat transfer rates, as discussed more in details in (Moallem et al., 2012a) (Moallem et al., 2012b).

When frost started to deposit on the surface it formed a frost layer with a considerable thickness on the fin surface, as shown in Figure 4. The air pressure drop across the microchannel increased considerably (Moallem et al., 2012c). With increasing pressure drop, the total air flow rate was affected and the air face velocity on the microchannel sample decreased. For every value of air pressure drop across the microchannel sample during the frosting test, one value of corresponding air face velocity was measured. The objective of the correlation developed in the present study was to correlate the change of the air face velocity entering the microchannel sample with frost thickness, fin geometric dimensions, and time, as shown in equations (9) to (12).

$$\text{Normalized Velocity}_{(\text{correlation})} = \frac{V_{air,face}}{V_{air,face_0}} = aFo_m{}^2 + bFo_m + 1 \quad (9)$$

$$a = (c_1 Ch_w^2 + c_2 Ch_{w+} c_3)(c_4 Ch_h^2 + c_5 Ch_h + c_6)(c_7 Ch_d^2 + c_8 Ch_{d+} c_9)(Fs)^{p_1} \quad (10)$$

$$p_1 = (c_{10} Ch_w^2 + c_{11} Ch_{w+} c_{12})(c_{13} Ch_h + c_{14})(c_{15} Ch_d^2 + c_{16} Ch_{d+} c_{17}) \quad (11)$$

$$b = (c_{18} Ch_w^2 + c_{19} Ch_{w+} c_{20})(c_{21} Ch_h^2 + c_{22} Ch_h + c_{23})(c_{24} Ch_d^2 + c_{25} Ch_{d+} c_{26})(Fs)^{c_{27}} + c_{28} \quad (12)$$

In the above equations, a and b are function of fin geometry and Fs number and p_1 is the power of frost umber. There are a set of constant which are shown in Table 4. Ch_h, Ch_w and Ch_d are in mm. The present form of velocity correlation predicted the velocity reduction on the 7 different geometries with three different surface temperatures. The result for microchannel sample 6 is shown in Figure 6. Similar results were obtained for other samples (see Figure 7). The overall performance of velocity correlation in equation (9) is shown in Figure 7. There is a concentration of data points on the right side of the horizontal axis where the normalized experimental air face velocity is near 1. Figure 7 also shows that near the end of the test where the air velocities are low the error percentage increases. These points were the points when the velocities were very low. As shown in Figure 6, while the correlation does not fail to predict the experimental data at the end of each frost test, the magnitude of velocity is small and a large percentage of error occurs.

Table 4: Coefficients of geometry in general frost air face velocity correlation

c1	2.36032E-02	c6	5.90549E-08	c11	9.29921E-01	c16	1.12464E-01	c21	4.46048E-03	c26	-7.70151E+01
c2	-5.50886E-01	c7	9.37121E-04	c12	-3.22532E+00	c17	-1.92793E-01	c22	-6.67660E+00	c27	2.50000E+00
c3	3.74068E+00	c8	-3.02470E-02	c13	-3.31519E-01	c18	-2.08972E-06	c23	9.30292E+00	c28	6.00000E-05
c4	2.22105E-08	c9	1.24149E+00	c14	2.40261E+00	c19	4.74618E-05	c24	-1.22558E-01		
c5	-7.95832E-08	c10	-4.68794E-02	c15	-2.63953E-03	c20	-2.55006E-04	c25	6.16741E+00		

Figure 7 shows that the concentration of data point is not uniform all through the horizontal axis. The data points have been collected in equal time intervals in the frost test. However since for considerable time of the test, the air velocity is near initial velocity as shown in Figure 6, the concentration of data point are grouped more around 1 in the horizontal axis of Figure 7. A small percentage of the data points were located outside 10% accuracy of the present correlation according to the following analysis. Table 5 provide a summary of the statistical error when using the correlation (9) for predicting the experimental velocity data, The errors in Table 5 are calculated for 375 data points in 21 frost tests for 7 geometries of the present study; each geometry was run at three different fin surface temperature. The error was calculated in the same method described before regarding the thickness correlation. Data shows that velocity correlation can predict the entire set of data with an average error of 7.7%.

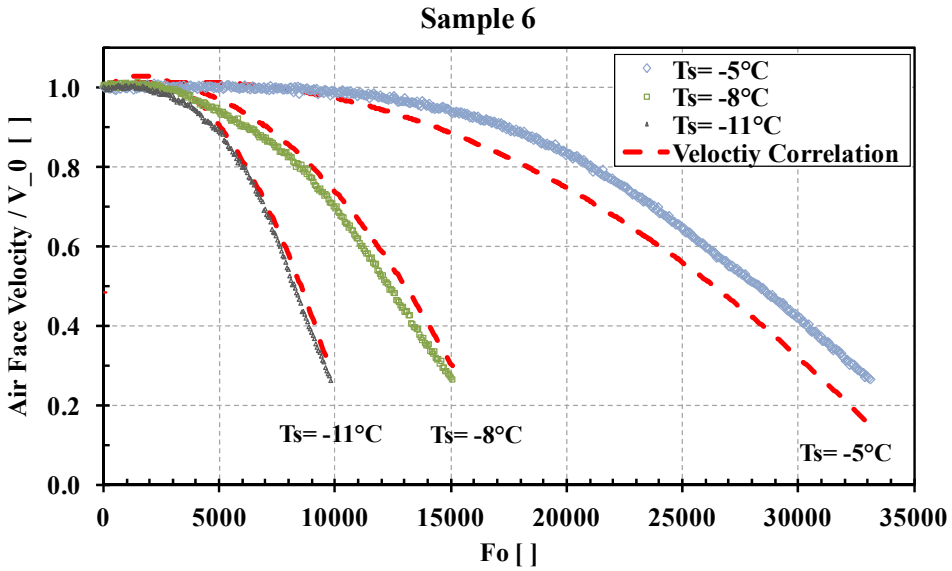

Figure 6: Air face velocity drop correlation vs. experimental measured air face velocity data Sample 6. Similar results were observed for other samples.

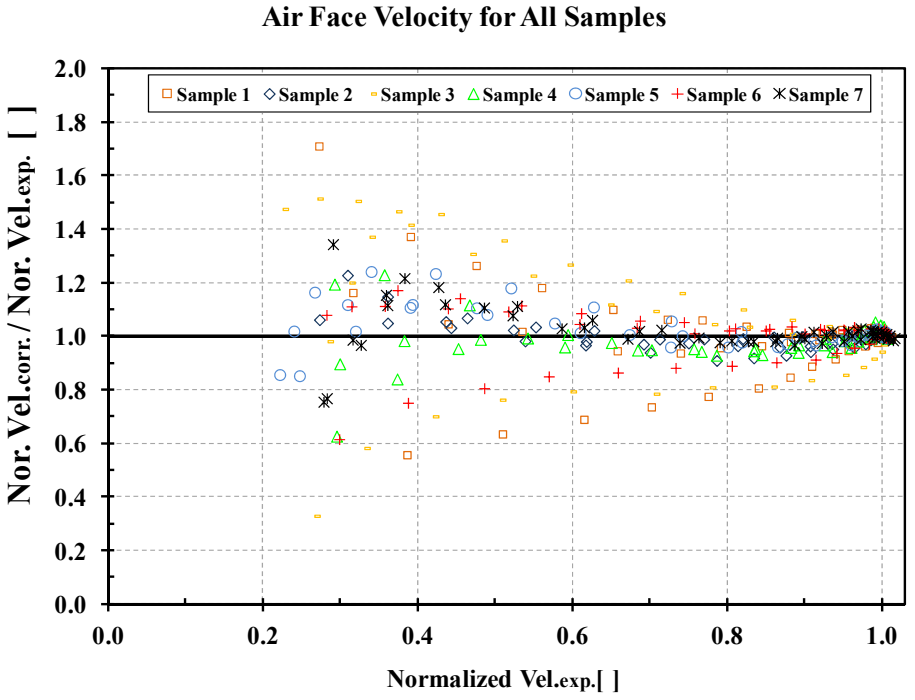

Figure 7: Frost air face velocity correlation versus normalized experimental measured air face velocity data for Samples 1 ~ 7.

Sample No./ Bank	Nor. Air Vel. predicted w ithin average of ± [%]	RMS Error [%]
Sample 1	9.2	50.4
Sample 2	3.1	21.5
Sample 3	21.6	34.7
Sample 4	4.6	38.8
Sample 5	4.8	28.4
Sample 6	6.2	28.2
Sample 7	4.7	13.4
80% of Entire Data Base	3.9	-
95% of Entire Data Base	6.2	-
Entire Data Base	**7.7**	12.3

Table 5: Velocity Correlation overall performance

The rate of change of the air face velocity did not depend only on air pressure drop through the microchannel but also on the fan curve and the system resistance due to the duct and other components of the test set up. In the present study, the blower used during the experiments was representative of a mid class well sized fan with a near linear curve characteristic within the range of testing operating conditions. When the pressure drop increased, the flow dropped linearly and similar behavior is expected for an actual fan-coils assembly in air-source heat pumps. It should be noted that only a small part of total air flow (about 5 cfm or 0.0024 m^3/s) was diverted to the small microchannel samples while the rest of flow (about 100 cfm or 0.047 m^3/s) was recirculated and bypassed the fin sample. Thus, when reducing 5 cfm (0.0024 m^3/s) to the sample to zero cfm, the rest of flow was practically unaffected and the working conditions of the fan in the test set up were not drastically influenced during the frosting tests of the present work. From this perspective, the authors concluded that the data obtained in the present study on air face velocity reduction were practically independent from the fan used in the test set up. It was clear that the change of air velocity were mainly due to the behavior of the fins geometry during their frost buildups. . It is worth to emphasize that all of the equations mentioned in this section, equations (4) to (12), are explicit equations that can be setup using a spreadsheet to predict the value of frost thickness and air velocity at each time during the frost period. These values can be used to calculate the instantaneous Re number for prediction of the heat transfer coefficient. Future studies might be required to extend the frost and velocity reduction correlation to a broader range of fin geometry and operating conditions, specifically for a larger set of ambient temperatures and humidity.

4. CONCLUSIONS

The present work focused on various aspects of frost formation on louvered folded fins in outdoor microchannel heat exchangers used in air source heat pump systems. More than 90 tests with different surface temperatures were performed on 7 microchannel fin samples with different geometry and the effects of surface temperature, fin geometries on the thermal and hydraulic performance of the microchannel heat exchangers under frosting conditions were studied. This paper presents new correlations for frost thickness and air face velocity reduction that properly account for frosting operating conditions of 7 fin geometries for microchannel heat exchangers. The developed correlations were verified for fin surface temperature ranging from -11°C (12°F) to -5°C (23°F) and were able to predict the frost thickness and air face velocity degradation within average error of ±17.6% and ±7.7%. Correlations that predict the frost thickness and the reduction of air face velocity during frosting operation can be used to calculate the instantaneous air-side Reynolds number during frosting operation of the fins, which is a fundamental parameter for predicting the heat transfer rates of the microchannel coils in quasi-steady state frosting operating conditions.

NOMENCLATURE

Ch_d or C_d: Channel depth (air side) or Coil depth (mm)
Ch_h: Channel height (air side) (free space between two adjacent fins) (mm)
Ch_w: Channel width (air side) (free apace between two adjacent vertical tube walls) (mm)
D_{ab}= binary diffusion coefficient of water to air (2.28E-5) (m2/s)
Fo or Fo_m: mass transfer Fourier number (eq. 5)
Fs: Frost number or supersaturation level of air (eq. 1)
l_l: Louver length (mm)
l_p or L_p: Louver pitch (mm)
$\dot{m}$: mass flow rate (kg/s)
P_{air}: Pressure of water vapor pressure in the air stream (Pa)
P_{surf}: Pressure of water vapor pressure in the air at surface temperature (Pa)
t : (Frost) thickness (m)
t_{fin}: fin thickness (m)
t_t: time (sec)
T : Temperature (°C)
V: Velocity (m/s)

Greek letters

δ : dim. less frost thickness ( )
ω: absolute air humidity (kg/kg)

Subscripts

0 : at initial time (t=0)
f : frost
s, surf: surface

REFERENCES

AHRI. (Standard 210/240, 2008), Performance Rating of Unitary Air Conditioning and Air-Source Heat Pump Equipment, Air Conditioning, Heating and Refrigeration Institute.

Garimella, S., 2003, Innovations in energy efficient and environmentally friendly space-conditioning systems, *Energy,* vol. 28: P. 1593-1614.

Hoke, J. L., Georgiadis, J. G., Jacobi, A. M., 2004, Effect of substrate wettability on frost properties, *Journal of Thermophysics and Heat Transfer*, vol. 18: P. 228-235.

Hong, T., 2011, Measurements of Frost Growth on Louvered Folded Fins of Microchannel Heat Exchangers, *Mechanical & Aerospace Engineering, Oklahoma State University*, Stillwater, OK, USA.

Hong, T., Moallem, E., Cremaschi, L., Fisher, D., 2012, Measurements of Frost Growth on Louvered Folded Fins of Microchannel Heat Exchangers, Part 1: Experimental Methodology. *ASHRAE Transactions*, vol. 118: (Preprint under preparation).

Kim, J.-H., Groll, E. A., 2003, Microchannel Heat Exchanger Defrost Performance and Reliability. *ASHRAE final report*, 1195-RP, Atlanta, GA, USA.

Kim, M.-H., Bullard, C.W., 2002, Performance Evaluation of a Window Room Air Conditioner With Microchannel Condensers. *Journal of Energy Resources Technology*, vol. 124: P. 47-55.

Kondepudi, S.N., O'Neal, D.L. 1989, Effect of frost growth on the performance of louvered finned tube heat exchangers. *International Journal of Refrigeration*, vol. 12: P. 151-158.

Lee, K.-S., Kim, W.-S., Lee, T.-H., 1997, A one-dimensional model for frost formation on a cold flat surface. *International Journal of Heat and Mass Transfer*, vol. 40: P. 4359-4365.

Moallem, E., Cremaschi, L., Fisher, D.E. 2010, Experimental Investigation of Frost Growth on Microchannel Heat Exchangers. *International Refrigeration and Air Conditioning Conference at Purdue University*, West Lafayette, IN, USA, July 12-15, 2010.

Moallem, E., Padhmanabhan, S., Cremaschi, L., Fisher, D.E., 2012a, Experimental investigation of the surface temperature and water retention effects on the frosting performance of a compact microchannel heat exchanger for heat pump systems. *International Journal of Refrigeration*, vol. 35: P. 171-186.

Moallem, E., Cremaschi, L., Fisher, D.E., Padhmanabhan, S., 2012b, Experimental measurements of the surface coating and water retention effects on frosting performance of microchannel heat exchangers for heat pump systems. *Experimental Thermal and Fluid Science*, vol. 39: P. 176-188.

Moallem, E., Hong, T., Cremaschi, L., Fisher, D.E., 2012c, Experimental Investigation of Adverse Effect of Frost Formation on Microchannel Evaporators, Part 1: Effect of Fin Geometry and Environmental Effects. *International Journal of Refrigeration* (Under Review).

Moallem, E., Hong, T., Cremaschi, L., Fisher, D.E., Deokar, P., 2012d, Effect of Fin Design on Frost and Defrost Thermal Performances of Microchannel Heat Exchangers, in: 1589-RP (Ed.), *ASHRAE Final Report*.

Na, B., Webb, R.L., 2003, A fundamental understanding of factors affecting frost nucleation. *International Journal of Heat and Mass Transfer*, vol. 46: P. 3797–3808.

Na, B., Webb, R.L., 2004, Mass transfer on and within a frost layer. *International Journal of Heat and Mass Transfer*, vol. 47: P. 899-911.

Padhmanabhan, S., Fisher, D.E., Cremaschi, L., Knight, J., 2008, Comparison of frost and defrost performance between microchannel coil and fin-and-tube coil for heat pump systems. *12th International Refrigeration and Air Conditioning Conference* at Purdue West Lafayette, IN, USA, paper no. R2202.

Park, C.Y., Hrnjak, P., 2007, Effect of heat conduction through the fins of a microchannel serpentine gas cooler of transcritical CO2 system. *International Journal of Refrigeration*, vol. 30: P. 389-397.

Sanders, C.T., 1974, The influence of frost formation and defrosting on the performance of air coolers, *Ph.D. Thesis, Technische Hogeschool*, Delft, Netherlands.

Shin, J., Tikhonov, A.V., Kim, C., 2003, Experimental study on frost structure on surfaces with different hydrophilicity: density and thermal conductivity. *ASME Journal of Heat Transfer*, vol. 125: P. 84-94.

Thomas, L., Chen, H., Besant, R.W., 1999, Measurement of frost characteristics on heat exchanger fins, part I: test facility and instrumentation., *ASHRAE Transactions*, vol. 105: P. 283-293.

Xia, Y., Zhong, Y., Hrnjak, P.S., Jacobi, A.M., 2006, Frost, defrost, and refrost and its impact on the air-side thermal-hydraulic performance of louvered-fin, flat-tube heat exchangers, *International Journal of Refrigeration*, vol. 29: P. 1066-1079.

Zhang, P., Hrnjak, P.S., 2010, Air-side performance of a parallel-flow parallel-fin (PF2) heat exchanger in sequential frosting. *International Journal of Refrigeration*, vol. 33: P. 1118-1128.

ACKNOWLEDGEMENT

The authors gratefully acknowledge funding and support from ASHRAE as well as the help of the Project Monitor Subcommittee Members and ASHRAE Technical Committee TC 8.4 Air-to-refrigerant Heat Transfer Equipment.
The authors would also like to thank Pratik Deokar, a graduate student from Oklahoma State University, for the help with performing some of the tests, the service and maintenance of the test facility.